

AUTHOR QUERY FORM

	Journal: HE Article Number: 11778	Please e-mail or fax your responses and any corrections to: E-mail: corrections.essd@elsevier.tnq.co.in Fax: +31 2048 52789
---	--	---

Dear Author,

Please check your proof carefully and mark all corrections at the appropriate place in the proof (e.g., by using on-screen annotation in the PDF file) or compile them in a separate list. Note: if you opt to annotate the file with software other than Adobe Reader then please also highlight the appropriate place in the PDF file. To ensure fast publication of your paper please return your corrections within 48 hours.

For correction or revision of any artwork, please consult <http://www.elsevier.com/artworkinstructions>.

Any queries or remarks that have arisen during the processing of your manuscript are listed below and highlighted by flags in the proof.

Location in article	Query / Remark: Click on the Q link to find the query's location in text Please insert your reply or correction at the corresponding line in the proof
Q1	<p>Please confirm that given names and surnames have been identified correctly.</p> <div style="border: 1px solid black; padding: 5px; margin-top: 10px;"> <p>Please check this box or indicate your approval if you have no corrections to make to the PDF file</p> <input type="checkbox"/> </div>

Thank you for your assistance.



ELSEVIER

Available online at www.sciencedirect.com**SciVerse ScienceDirect**journal homepage: www.elsevier.com/locate/he

Graphical Abstract

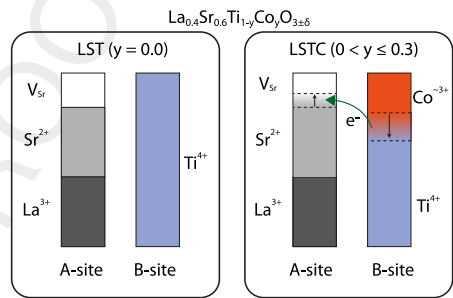
International Journal of Hydrogen Energy 2013, ■, ■■■

Electronic and structural properties of $\text{La}_{0.4}\text{Sr}_{0.6}\text{Ti}_{1-y}\text{Co}_y\text{O}_{3\pm\delta}$ electrode materials for symmetric SOFC studied by hard X-ray absorption spectroscopy

Federico Napolitano ^{a,*}, Analía L. Soldati ^a, Jochen Geck ^b, Diego G. Lamas ^c, Adriana Serquis ^a

^a CONICET – CNEA Departamento de Caracterización de Materiales, Centro Atómico Bariloche, Av. Bustillo 9500, San Carlos de Bariloche R8402AGP, Río Negro, Argentina

^b Leibniz Institute for Solid State and Materials Research IFW Dresden, 01069 Dresden, Germany



Highlights

- XANES/EXAFS reveal invariance of the local structure and formal valence of Ti in LSTC.
- Dramatic changes at the Co-site are produced with increasing Co content.
- Stability of Ti⁴⁺ triggers the formation of A-site vacancies in LSTC materials.
- The reduction of A-site deficiency with increasing Co content in LSTC is explained.
- An improved electrochemical performance for higher Co content is predicted.



ELSEVIER

Available online at www.sciencedirect.com**SciVerse ScienceDirect**journal homepage: www.elsevier.com/locate/he

Electronic and structural properties of $\text{La}_{0.4}\text{Sr}_{0.6}\text{Ti}_{1-y}\text{Co}_y\text{O}_{3\pm\delta}$ electrode materials for symmetric SOFC studied by hard X-ray absorption spectroscopy

^a **Federico Napolitano**^{a,*}, **Analía L. Soldati**^a, **Jochen Geck**^b, **Diego G. Lamas**^c,
Adriana Serquis^a

^a CONICET – CNEA Departamento de Caracterización de Materiales, Centro Atómico Bariloche, Av. Bustillo 9500, San Carlos de Bariloche R8402AGP, Río Negro, Argentina

^b Leibniz Institute for Solid State and Materials Research IFW Dresden, 01069 Dresden, Germany

^c CONICET, Laboratorio de Caracterización de Materiales, Facultad de Ingeniería, Universidad Nacional del Comahue, Buenos Aires 1400, 8300 Neuquén Capital, Neuquén, Argentina

ARTICLE INFO

Article history:

Received 18 February 2013

Received in revised form

11 April 2013

Accepted 1 May 2013

Available online xxx

Keywords:

LSTC

XANES

EXAFS

Symmetrical SOFC electrode

ABSTRACT

We present combined Synchrotron X-ray Absorption Near Edge Spectroscopy (XANES) and Extended X-ray Absorption Fine Structure (EXAFS) study of $\text{La}_{0.4}\text{Sr}_{0.6}\text{Ti}_{1-y}\text{Co}_y\text{O}_{3\pm\delta}$ ($0 \leq y \leq 0.5$), which are promising electrode materials for symmetric solid oxide fuel cells. The measurements were performed at room temperature at the Ti and the Co K-edges in order to determine the local structural and electronic changes around the two transition metals. We find that Ti remains in a higher formal valence (around 4+) independent of the Co concentration. In contrast to this, dramatic and systematic changes are observed for the Co as a function of y. We conclude that the stability of the Ti^{4+} triggers the A-site deficiency in our samples and predicts that oxygen vacancies are much more easily formed at large Co content, which in turn will greatly enhance the performance as electrode material.

Copyright © 2013, Hydrogen Energy Publications, LLC. Published by Elsevier Ltd. All rights reserved.

1. Introduction

ABO_3 perovskites with Ti in the B site are promising electrode materials for a new subtype of Solid Oxide Fuel Cells (SOFC), the so called Symmetrical SOFC (SSFOC), reported for first time by Ruiz-Morales et al. [1,2]. SSFOC are based on a symmetric design where the same compound is used as cell anode and cathode. Advantages over traditional SOFC relies on their simpler design, dealing with compatibility and inter-diffusion problems between cell components and even helping to

manage the anode sulfur and carbon poisoning by simply reversing the gas flux, issues that strongly affects SOFC anodes long term efficiency.

Perovskites belonging to the $\text{La}_x\text{Sr}_{1-x}\text{TiO}_3$ (LST) family are recognized for their good properties in a SOFC anode reductive environment [3]. Besides, the replacement of small amounts of Ti with other transition metals can enhance their ionic and electronic conductivity in oxidizing atmospheres, therefore, enabling the use of doped LST as possible SOFC cathodes [4,5]. Attending the wide experience gained with the $\text{La}_{1-x}\text{Sr}_x\text{CoO}_{3-\delta}$

* Corresponding author. Tel.: +54 2944 445100x5389; fax: +54 2944 445100x5283.

E-mail addresses: napolit@ib.cnea.gov.ar (F. Napolitano), asoldati@cab.cnea.gov.ar (A.L. Soldati), j.geck@ifw-dresden.de (J. Geck), diego.lamas@fain.uncoma.edu.ar (D.G. Lamas), aserquis@cab.cnea.gov.ar (A. Serquis).
0360-3199/\$ – see front matter Copyright © 2013, Hydrogen Energy Publications, LLC. Published by Elsevier Ltd. All rights reserved.
<http://dx.doi.org/10.1016/j.ijhydene.2013.05.005>

131
132
133
134
135
136
137
138
139
140
141
142
143
144
145
146
147
148
149
150
151
152
153
154
155
156
157
158
159
160
161
162
163
164
165
166
167
168
169
170
171
172
173
174
175
176
177
178
179
180
181
182
183
184
185
186
187
188
189
190
191
192
193
194
195
196
197
198
199
200
201
202
203
204
205
206
207
208
209
210
211
212
213
214
215
216
217
218
219
220
221
222
223
224
225
226
227
228
229
230
231
232
233
234
235
236
237
238
239
240
241
242
243
244
245
246
247
248
249
250
251
252
253
254
255
256
257
258
259
260

(LSC) as mixed conductor for SOFC cathodes [6,7] and the support of theoretical calculations [8], the substitution of Ti by Co atoms seems to be an adequate way to enhance LST mixed conductivity.

However, substitution of atoms with other valences in the ABO_3 structure might induce oxidation and reduction processes in the components or even creation of vacancies in the oxygen or the A-site sublattice, in order to compensate for charge and size changes [9]. Some authors reported that doping SrTiO_3 with $3+$ ions on the perovskite A-site may increase the oxygen non-stoichiometry, creates A-site deficiency and/or changes the ratio of Ti^{4+} to Ti^{3+} thus enhancing the conductivity. The predominance of one of these compensating mechanisms depends on synthesis temperature and reducing conditions [3,10]. The already mentioned replacement of Ti^{4+} on the perovskite B-site can also alter the structural properties of the titanates [11,12]. Therefore, substitutions may not only affect the electrochemical behavior, but also the material structure itself. An important requirement in the optimization of doped titanates as SSOFC electrodes is to identify and understand the active charge compensation mechanisms and their influence over structural parameters and electronic configuration. For example: A-site deficiency is related to phase stability [10] and to mixed conductivity [13], O vacancies strongly influences ionic conductivity [6] and the transition metal (TM) oxidation state affects the electronic conductivity [11].

In a previous work we investigated the series $\text{La}_x\text{Sr}_{1-y}\text{Ti}_{1-y}\text{Co}_y\text{O}_{3\pm\delta}$ (LSTC) with $x = 0.4$ and y varying between 0.0 and 0.5 [14]. A structural characterization using high resolution synchrotron X-ray Powder Diffractometry (XPD) and Transmission Electron Microscopy (TEM) methods showed that the creation of Sr vacancies at the A-site is the main compensation mechanism for charge and size changes, and that the A-site vacancies concentration decreases with the incorporation of Co in the crystal structure. The existence of Sr segregation in samples with A-site deficiency was supported by the presence of an amorphous background in the XPD data and local crystallinity loss observed by TEM. The physical reason for the creation of A-site vacancies, however, remained to be clarified. Simultaneously, the characterization

of $\text{La}_{0.5}\text{Sr}_{0.5}\text{Ti}_{0.5}\text{Co}_{0.5}\text{O}_{3-\delta}$ through neutron diffraction measurements was reported [15], indicating that this compound is fully stoichiometric at room temperature and presented a different space group than our samples (i.e., for $y = 0.5$ and $x = 0.5$, this work reported a crystal structure corresponding to the orthorhombic Pbnm space group, while for a similar composition, $y = 0.5$ and $x = 0.4$, our best fit of XPD data was obtained assuming the R-3c rhombohedral space group).

We concluded from our previous studies that the presence of Co, which should modify its oxidation state more easily than Ti, might preclude the formation of A-site vacancies, even at low synthesis temperature. However, the lack of published data on the electronic properties of the B-site transition metals in this series made it impossible to validate that assumption. Moreover, the knowledge of the electronic configuration of the B-sites is crucial in order to understand the electrochemical properties of SSOFC electrodes.

In this work, we experimentally investigate the electronic configuration, oxidation state and nearest neighbors coordination behavior of cobalt and titanium in the same samples and tested our previous hypothesis using synchrotron X-ray Absorption techniques. These results will help to establish and characterize the LSTC charge compensation mechanisms and understand the physical origin of the electrochemical properties of these materials as SOFC electrode.

2. Experimental method

2.1. Samples and synthesis method

Samples with nominal compositions of $\text{La}_{0.4}\text{Sr}_{0.6}\text{Ti}_{1-y}\text{Co}_y\text{O}_{3\pm\delta}$ with $0 \leq y \leq 0.5$ (LSTC) were prepared by a citrate chemical route. Ti(IV) -butoxide, La_2O_3 , SrCO_3 , and $\text{Co}(\text{NO}_3)_2$ were used as precursor materials; they were mixed in different ratios to get the desired compositions and the formed sol-gel was then calcinated at 300°C . More details about this synthesis are reported elsewhere [14]. The as-prepared powders were sintered at 750°C and at 1100°C (Table 1) with grain sizes of about 40 and 500 nm, respectively, in order to study possible grain size effects. Desired phase formation, without traces of

Table 1 – Results from XANES and EXAFS analyses of $\text{La}_{0.4}\text{Sr}_{0.6}\text{Ti}_{1-y}\text{Co}_y\text{O}_{3\pm\delta}$ samples ($0.0 \leq y \leq 0.5$) synthesized at 750 and 1100°C . T_s: Sintering temperature; O.S.: Oxidation state; R₁: first coordination sphere distance to transition metal; σ²: Debye-Waller factor.

Sample name	y	Nominal composition	T _s (°C)	XANES			EXAFS		
				O.S. _{Co}	O.S. _{Ti}	R ₁ Co (Å)	σ ² Co (Å ²)	R ₁ Ti (Å)	σ ² Ti (Å ²)
LSTC00-750	0.0	$\text{La}_{0.4}\text{Sr}_{0.6}\text{TiO}_{3\pm\delta}$	750	—	4.0	—	—	—	—
LSTC01-750	0.1	$\text{La}_{0.4}\text{Sr}_{0.6}\text{Ti}_{0.9}\text{Co}_{0.1}\text{O}_{3\pm\delta}$	750	2.5	4.0	2.02 (1)	0.005	1.91 (1)	0.003
LSTC02-750	0.2	$\text{La}_{0.4}\text{Sr}_{0.6}\text{Ti}_{0.8}\text{Co}_{0.2}\text{O}_{3\pm\delta}$	750	2.5	4.0	—	—	—	—
LSTC03-750	0.3	$\text{La}_{0.4}\text{Sr}_{0.6}\text{Ti}_{0.7}\text{Co}_{0.3}\text{O}_{3\pm\delta}$	750	2.7	4.0	1.95 (1)	0.007	1.91 (1)	0.002
LSTC04-750	0.4	$\text{La}_{0.4}\text{Sr}_{0.6}\text{Ti}_{0.6}\text{Co}_{0.4}\text{O}_{3\pm\delta}$	750	3.1	4.0	—	—	—	—
LSTC05-750	0.5	$\text{La}_{0.4}\text{Sr}_{0.6}\text{Ti}_{0.5}\text{Co}_{0.5}\text{O}_{3\pm\delta}$	750	3.1	4.0	1.92 (1)	0.007	1.89 (1)	0.0002
LSTC00-1100	0.0	$\text{La}_{0.4}\text{Sr}_{0.6}\text{TiO}_{3\pm\delta}$	1100	—	4.0	—	—	—	—
LSTC01-1100	0.1	$\text{La}_{0.4}\text{Sr}_{0.6}\text{Ti}_{0.9}\text{Co}_{0.1}\text{O}_{3\pm\delta}$	1100	2.4	4.0	2.04 (1)	0.004	1.91 (1)	0.004
LSTC03-1100	0.3	$\text{La}_{0.4}\text{Sr}_{0.6}\text{Ti}_{0.7}\text{Co}_{0.3}\text{O}_{3\pm\delta}$	1100	2.6	4.0	1.95 (1)	0.006	1.91 (1)	0.002
LSTC05-1100	0.5	$\text{La}_{0.4}\text{Sr}_{0.6}\text{Ti}_{0.5}\text{Co}_{0.5}\text{O}_{3\pm\delta}$	1100	3.3	4.0	1.92 (1)	0.005	1.91 (1)	0.0001

secondary phases, was verified on all samples through laboratory and synchrotron X-ray Diffraction.

2.2. X-ray absorption spectroscopy (XAS)

XAS measurements at the Co and Ti K-edges were carried out in the DB04-XAFS beamline of the Brazilian Synchrotron Light Laboratory, LNLS, Campinas, Brazil. Synthesized samples as well as Co and Ti reference materials, were measured in transmission mode at room temperature. XAS samples were discs of 1 cm diameter prepared by mixing LSTC materials with BN powder in a ratio of approximately 1:5, which were compacted by uniaxial pressing. The mass of LSTC was calculated in order to obtain a total absorption above the edge of 1.5 (i.e. $\mu t = 1.5$, where μ and t are the linear absorption coefficient and the effective thickness, respectively). A Si (1 1 1) crystal was used as monochromator and was scanned from 200 eV below to 1200 eV above the K absorption edges of Co and Ti. Energy steps of 0.5 and 2 eV were used for the XANES and EXAFS regions, respectively. Three spectra were averaged each time for the signal-to-noise ratio optimization for most measurements. The energy reproducibility between measurements was better than 0.1 eV at the K-edge, as determined using the metal references. A metallic foil (Ti or Co) was used in each case as a reference to calibrate for possible energy shifts. The foil and the $I_{\text{reference}}$ detector were placed behind the sample along the direction of X-ray beam. Reference materials comprised metallic Co (Co^0), LaCoO_3 (Co^{3+}) and BaCoO_3 (Co^{4+}) for cobalt and metallic Ti (Ti^0), LaTiO_3 , SrTiO_3 and TiO_2 (Ti^{4+}) for titanium.

The data reduction was done with Athena® and WinXAS® software. Energy calibration was applied setting the first maximum of the first derivative of the metallic reference foil equal to 7709.0 eV and 4966.0 eV for Co and Ti, respectively. The background was subtracted after fitting with two polynomials, one of first order for the pre-edge and the other of second order for the post-edge. The baseline-subtracted spectra were normalized to an intensity of one at the energy where no more EXAFS oscillations were detected. The edge position was calculated as the position of the first intense maximum of the first derivative curve of the normalized absorption spectrum.

WinXAS software was also used for EXAFS data refinement via the theoretical model approach. EXAFS signals were extracted in the range $3 \text{ \AA}^{-1} \leq k \leq 12 \text{ \AA}^{-1}$ using cubic splines and k^3 weighting following the procedure described elsewhere [16]. Their Fourier Transform (FT) was calculated using a Bessel window between the first and last well defined zero crossing. The well-known crystal structures of SrTiO_3 [17] and LaCoO_3 [18] perovskite-type oxides (both corresponding to the Pm-3m space group) were used as reference models for simulating the X-ray absorption scattering paths with the FEEF8.20 code [16]. This calculated data was then used as input for the refinement of the FT EXAFS signals in the R-space to calculate the bond distances for Ti and Co. Refinements were performed in the $1.1 \text{ \AA} \leq R \leq 1.9 \text{ \AA}$ in order to include only the first coordination sphere of the transition metals. The coordination numbers were fixed at 6 since it is not expected an appreciable oxygen deficiency for these samples as discussed later (synthesized in air at low temperatures and measured at room temperature).

3. Theory

The main purpose of the density functional theory (DFT) calculations performed in this study is to estimate the effects of purely structural changes on the Co K-edge XANES. To achieve this, the calculations were done for stoichiometric LaCoO_3 , using the structural data determined experimentally for our $\text{La}_{0.4}\text{Sr}_{0.6}\text{Ti}_{1-y}\text{Co}_y\text{O}_{3\pm\delta}$ ($y = 0.1, 0.3, 0.5$) samples [14]. In addition we also performed a calculation for structure with the lattice constants for $y = 0.1$ expanded by 2%. The DFT calculations were done in the local density approximation (LDA) using the Wien2K package [19] with $7 \times 7 \times 7$ k-points in the irreducible part of the Brillouin zone. For the simulation of the TM K-edge spectra, the total 4p density of states (DOS) was calculated by DFT first. Since we are dealing with powder samples, the total 4p DOS was used, which corresponds to a sum over different crystal directions. The 4p DOS was then broadened by 1 eV in order to take into account the experimental resolution as well as the core-hole life time and shifted by 7709 eV in order to facilitate comparison with experiment. Note that, in this approximation, only the dominant $1s \rightarrow 4p$ dipole transitions are considered, whereas the much weaker $1s \rightarrow 3d$ quadrupole transitions are neglected. Furthermore, the simulated XAS spectrum is based on the ground state charge density and as such neglects possible charge density excitations (screening, charge transfer) caused by the additional potential of the 1s core hole.

4. Results

4.1. XANES (X-ray near edge structure)

The absorption coefficient at the cobalt K-edge of the LSTC samples and the reference materials are shown in Fig. 1A. The

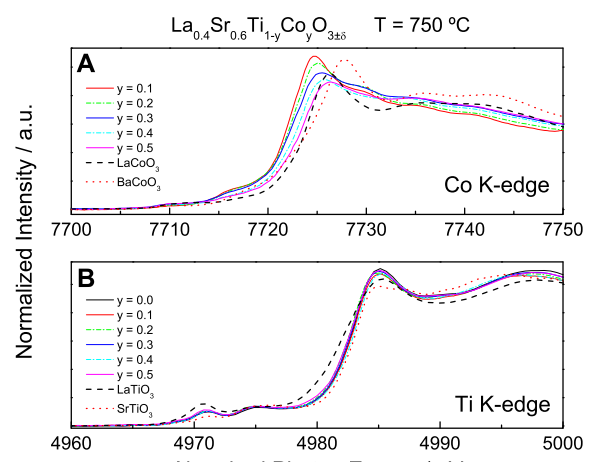


Fig. 1 – $\text{La}_{0.4}\text{Sr}_{0.6}\text{Ti}_{1-y}\text{Co}_y\text{O}_{3\pm\delta}$ ($0.0 \leq y \leq 0.5$) normalized X-ray absorption spectra around Co (A-top) and Ti (B-bottom) K-edge absorption edge for samples synthesized at 750 °C. Standard samples with a well-known transition metal oxidation state are also drawn (dashed lines) for the purpose of comparison.

main absorption jump can be observed in all cobalt spectra between 7705 and 7725 eV. This peak is known as the "white line" (WL) and is due to strong $1s \rightarrow 4p$ electric dipole transitions. In the following we will also define the edge position E_0 as the first peak in the first derivative of the XANES spectra (the point with the steepest slope). Regarding the LSTC series, two main changes of the Co K-edge XANES spectra can be recognized by increasing the doping fraction y : first, the edge position E_0 moves to higher energies and second, the WL decreases. In contrast to this, the Ti K-edge XANES spectra do not show any appreciable change as a function of y , as can be observed in Fig. 1B. In this case, the WL is located at 4985 eV while $E_0 = 4983$ eV. As it can be clearly seen in the figure, the Ti K-edge XANES spectra do not show any significant shift in position, staying close to the SrTiO_3 edge energy, which we take as Ti^{4+} reference. The direct comparison of the first derivatives for samples synthesized at 750 and 1100 °C (Fig. 2A and B, respectively) makes it evident that both LSTC series show the same behavior, independently of the grain size (given by the synthesis temperature).

It is commonly accepted that the position of the TM K-edges is, among other factors, related to the average valence of the absorber [20,21]. Indeed, a linear shift in the absorption threshold of the Co perovskite series from lower to higher energies upon oxidation has been reported [22–25].

This fact motivates the attempt to determine the oxidation state of Co as a function of y , by comparing the Co K-edge position of LSTC samples with that of own known reference materials in Fig. 2C. Several reported data (close symbols)

were also included as references to increase the calibration accuracy (open symbols). A linear regression (dotted line) resulted in the relation $Y = aX + b$ with $a = (2.1 \pm 0.2)$ eV and $b = (7713.3 \pm 0.6)$ eV. The unknown cobalt oxidation states of the samples were then estimated from the interpolation of the standard edge energy versus valence state linear fit. This calculation suggests formal oxidation states between 2.4 ± 0.1 and 3.3 ± 0.1 for LSTC samples with $0.1 \leq y \leq 0.5$ (see Table 1).

Following the same line of arguments, the XANES data for Ti K-edge provide evidence that the formal valence of Ti remains unchanged as a function of y . More specifically, since all the Ti K-edge energies agree with that of SrTiO_3 within the error of the experiment, our results indicate that the formal valence of Ti is close to $4+$ for all the LSTC samples.

The above interpretation of the K-edge position hence indicates that the oxidation state of Co changes as a function of y , while that of Ti remains fixed. However, care must be taken with interpreting the position of TM K-edges in terms of formal oxidation states. Since the 4p-states are quite extended they are also strongly influenced by structural changes, i.e., the edge shifts may not only be given by the valence of the absorber, but also by changes of the local atomic structure around the absorber.

4.2. B-site local environment (EXAFS)

In order to determine the significance of the changes in the local atomic structure around Co and Ti as a function of y , we performed extended x-ray absorption fine structure (EXAFS)

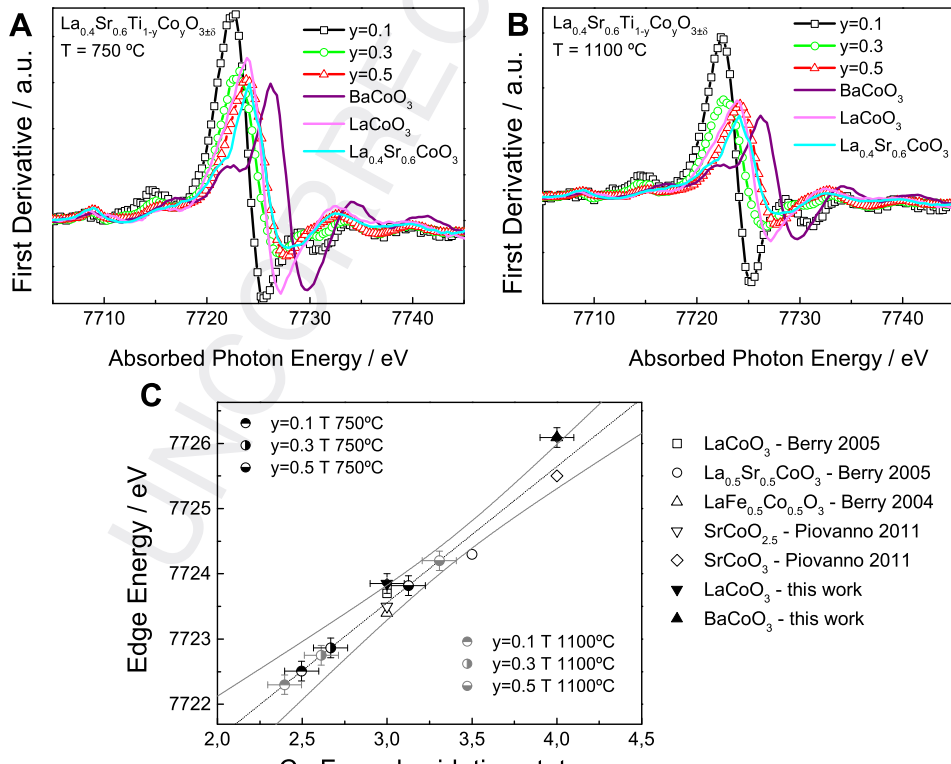


Fig. 2 – XANES spectra first derivative near Co absorption edge of $\text{La}_{0.4}\text{Sr}_{0.6}\text{Ti}_{1-y}\text{Co}_y\text{O}_{3\pm\delta}$ ($0.0 \leq y \leq 0.5$) synthesized at 750 °C (A) and 1100 °C (B). C) Calibration of XANES spectra edge energy position of standard samples with known Co oxidation state and determination of the Co oxidation state of our LSTC samples. Literature data were taken from references [22,37,38].

measurements at room temperature. This technique has the great advantage of allowing the study of the local structure around the absorber, which is much more difficult with other non-resonant techniques such as conventional X-ray diffraction. First EXAFS results are presented in Fig. 3 (a detailed local environment characterization of the LSTC series will be reported in a forthcoming publication), where the Fourier transform of the LSTC EXAFS signal and the refinements corresponding to the first coordination sphere around Co and Ti of the samples synthesized at 1100 °C is displayed. Similar results were obtained for samples synthesized at 750 °C (not shown). The Co–O distance decreases systematically with increasing y , from 2.02 to 1.92 Å, while the Ti–O distance remains constant at 1.91 Å (see Table 1) within the errors of the experiment. Typical Debye–Waller factors are in the range of 0.002–0.007 Å², which are expected for crystalline structures. These preliminary results further support the conclusion of our previous work: the TiO_6 and CoO_6 octahedra remain cubic with no noticeable distortion. In particular we find no evidence for a difference between Co-apical O and the others Co–O distances; this would be observed as a peak splitting in the first coordination sphere, which is not observed at the resolution of these experiments. The structural changes observed by XPD therefore seem not to be related to local symmetry reductions (i.e. distortions of the octahedra), but to a shrinking and tilting of essentially cubic octahedra.

EXAFS results in Fig. 3 are fully consistent with XANES results presented above: the constant Ti–O distances agree with the unchanged valence of Ti in the studied LSTC samples, whereas the strong changes observed for the Co–O are probably related to the change of the local electronic structure. Although the contraction of the Co–O distance with increasing y appears to be in line with an increased formal valence of Co, the observed change of about 0.1 Å is

surprisingly large and needs to be investigated in future dedicated experiments.

4.3. DFT theoretical calculations

EXAFS results indicate that the local structure around Co changes considerably with increasing y . In order to assess the influences of the local structure and to test the validity of the above analysis, which associates the shift of E_0 with a change in the Co valence, we performed DFT calculations. The simulated Co K-edge XANES spectra due to electric dipole transitions are displayed in Fig. 4. The first set of DFT calculations has been done for LaCoO_3 , using the averaged structures of $\text{La}_{0.4}\text{Sr}_{0.6}\text{Co}_y\text{Ti}_{1-y}\text{O}_{3\pm\delta}$ with $y = 0.1$ and 0.5 that were determined by XPD [14]. The Co–O distances in these cases were 1.962 Å and 1.937 Å, respectively. In addition we also performed calculations for hypothetical structures, where the lattice parameters for $y = 0.1$ were expanded by 4% and compressed by 2.1% in order to obtain the extreme Co–O distances 2.04 Å and 1.92 Å deduced from EXAFS. Note that these DFT models fix the formal valence of Co to 3+.

As it can be observed in Fig. 4, purely structural changes without any change in the Co valence already yield large shifts of the Co K-edge. From the average structure determined by XPD, the Co–O distance shrinks by about 0.025 Å with increasing y from 0.1 to 0.5, which yields a shift of E_0 of about 0.5 eV. Comparing this calculated shift to the observed value of about 2 eV, it can be concluded that the Co K-edge position mostly reflects a significant change of the Co valence. However, using the Co–O bond distances determined by EXAFS, which in contrast to XPD provides direct access to the local atomic structure around Co without long-range averaging, the Co–O bond length changes by about 0.12 Å. This large structural change causes a shift of the calculated E_0 that amounts

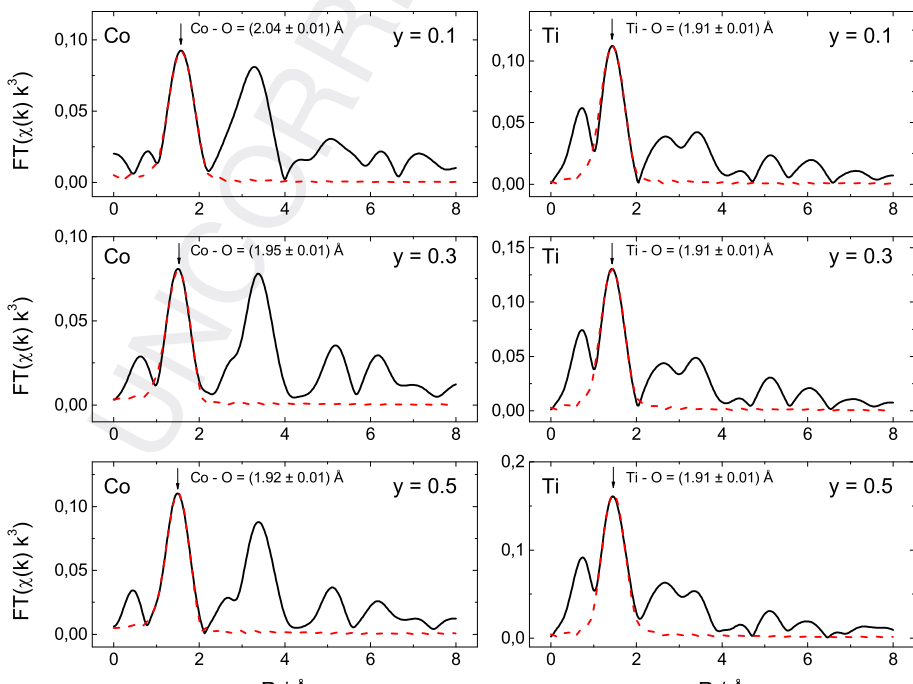


Fig. 3 – Fourier transform and first coordination sphere fit of LSTC samples. Cobalt (left) and titanium (right) EXAFS signals are shown for $y = 0.1, 0.3$ and 0.5 , respectively.

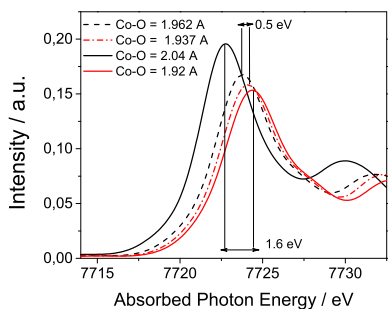


Fig. 4 – The p-projected Co-DOS as determined by DFT. The DOS is up-shifted by 7.709 keV and broadened by 1 eV, in order to facilitate comparison to the experimental data. Dashed lines show the calculations done for the structure determined by XPD, while the solid lines show the results obtained for the hypothetical structures, which reproduce the Co–O distances determined by EXAFS (further explanations are given in the text).

to 1.6 eV, which is close to the experimentally observed shift. Note that, in addition, the calculations also reproduce the reduction of the WL (see Fig. 1).

The DFT results presented in Fig. 4 imply that structural distortions have a large impact on the Co K-edge and need to be considered when interpreting the observed edge shifts. In fact, this should also be true for other TM K-edges. The present analysis shows that the position of the Co K-edge alone cannot be used to obtain a precise estimate of the Co valence, if the local Co environment changes significantly between the studied samples. This seems to be the case in the LSTC material.

In general, for a reliable determination of TM formal valences by means of their K-edge XANES analysis, the local atomic structure also needs to be monitored. In the present case, the development of an improved approach, which combines EXAFS, XANES and DFT on a more quantitative level, should enable to achieve a better determination of the Co valence in the future. Other alternative techniques such as neutron diffraction, X-ray Photoemission Spectroscopy (XPS) or Mössbauer Spectroscopy may serve for an independent validation. At this point the comparison to the reference materials only allows us to say that the Co valence is around 3+. While we do not exclude changes of Co valence as a function of y , the analysis shown in Fig. 2C, which yields the Co valence resumed in Table 1, will overestimate the maximal span of the actual Co valence.

Finally we would like to mention that the Co–O distances determined via EXAFS indicate a spin–state transition of Co. The strongly increased Co–O distance for $y = 0.1$ is typical for a high-spin (HS) state, whereas the reduced Co–O distance at $y = 0.3, 0.5$ agrees well with a low-spin (LS) state [26]. Possible spin state transitions in the LSTC materials are intriguing and are subject of our ongoing work.

5. Discussion

As mentioned in the introduction, there are three mechanisms which are discussed in the literature in relation to the

compensation of charge and size changes with doping in LSTC: (i) vacancies in the perovskite A-site, (ii) changes of the oxidation state of the perovskite B-site, or (iii) changes in the oxygen stoichiometry (usually through creation of oxygen vacancies).

Which of these mechanisms is active at least partially depends on the external conditions. For example, in LST materials (without the incorporation of Co) synthesized at high temperatures (~ 1500 °C) under a reductive atmosphere, a reduction of Ti from 4+ to 3+ to balance the replacement of Sr by La has been reported in order to explain its elevated electronic conductivity [27]. However, a different synthesis method for the same material yields A-site deficient compound, which shows that also this mechanism is active under certain conditions [9].

In our case, LST samples were prepared as stoichiometric $(A,A')BO_3$ perovskite but as a result an A-site deficient material has been obtained [14], in agreement with reported works for a low temperature synthesized LST under oxidizing atmosphere [28–30]. More specifically, there is strong evidence that there is a Sr-deficiency inside the LST material itself and that the missing Sr accumulates in disordered regions in-between the LST grains [14].

The present study of our LSTC series provides new insights, which enable to deduce the physical reasons for the A-site vacancy formation in LST-based materials: our results show that the oxidation state and the local coordination of Ti remain essentially unchanged with increasing y , whereas significant changes are observed at the Co-site. At the same time, our refinements of the XPD data show that the number of A-site vacancies decreases with substituting Ti by Co.

To explain this behavior, we first note that Ti^{4+} is very stable. This is not only supported by our Ti K-edge XANES measurements. It is also expected based on the electronic structure, because the Ti 3d-levels in $SrTiO_3$ are situated well above the Fermi level [27]. The reduction of Ti^{4+} , e.g. by replacing Sr by La, means that electrons are added to these 3d-levels, which costs a finite energy. Then, under certain conditions, it may be more favorable to form A-site vacancies in order to keep the B-site (Ti) valence close to 4+.

According to our Co K-edge XANES data, the Co valence is close to 3+. Therefore, the substitution of Ti by Co removes the restriction that the average formal valence of the B-site has to be 4+. As y increases, the average B-site valence $O.S.B = 3y + 4(1 - y)$ decreases from 4+ to 3+ and the number of A-site vacancies is expected to decrease accordingly. This is in perfect agreement with our experimental results shown in Fig. 5. Importantly, adding Co to the system is expected to create electronic states close to the Fermi level, to which electrons can be added or from which electrons can be extracted. This statement is also supported by four points conductivity measurements carried on LSTC samples with $y = 0$ and $y = 0.5$, where it was observed at least five orders of magnitude higher electrical conductivity in the sample with Co (i.e. $\sigma = 7 \times 10^{-5}$ S/cm and $\sigma = 18.7$ S/cm for $y = 0$ and $y = 0.5$ at 1000 °C under air, respectively). Hui et al. [31] also reported large changes in conductivity when adding Co to $SrTiO_3$ sample ($\sigma \sim 3 \times 10^{-4}$ S/cm for $SrTiO_3$ and $\sigma \sim 0.02$ S/cm for $SrTi_{0.95}Co_{0.05}O_3$ both at 800 °C under air).

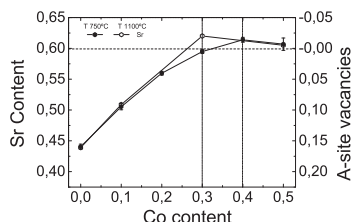


Fig. 5 – Evolution of strontium content, or equivalently A-site vacancies, as a function of Co content, determined from our previous X-ray diffraction study [14].

To further verify the model described above, we can estimate the number of A-site vacancies, assuming the following average occupation and formal valences: $A^{2.4+} \cdot D^{0.5} \cdot B^{3-}$. The assumed full occupation of the B- and O-site is justified by our refinements and previously published data [10,14]. For this simplified case, it follows immediately that $D = 0$ for a Co content of $y_c = 0.4$, which is in good agreement with the experimental data shown in Fig. 5, where the experimental value for y_c is found to be in the range of 0.3–0.4.

We therefore find that the formation of A-site vacancies in our LST-based materials is triggered by the stability of Ti^{4+} (cf. Fig. 6). Indeed, according to the arguments given above, it is very hard to create oxygen vacancies in LST, as this will add electrons to Ti and hence cost considerable energy. This situation should change dramatically when Co atoms replace Ti ones in LSTC, because now low energy electronic states at the Fermi level become available for the extra electrons introduced by oxygen deficiency. The presence of Co is therefore expected to enhance the materials ability to develop oxygen non-stoichiometry, which should greatly enhance the ionic conductivity of these compounds, as it was also observed in similar compounds [31,32].

This assertion is also supported by thermogravimetric weight loss (TG) used to determine the oxygen non-

stoichiometry (δ). These measurements were performed in a symmetrical thermo balance based on a Cahn 1000 electrobalance [33] coupled to an electrochemical system for the measurement and control of pO_2 [34] according to the procedure detailed in references [35] [36]. Measurements carried on LSTC samples with $y = 0, 0.3$ and 0.5 resulted in a mass loss of 0.1%, 0.6% and 0.8%, respectively, between room temperature and 800 °C under synthetic air. In addition, the δ variation at 800 °C between reductive (Ar) and oxidative (O_2) atmospheres is increased from 0.003 for $y = 0$ to 0.018 and 0.046 for 0.3 and 0.5 Co contents, respectively.

6. Conclusions

Our results show that in the $La_{0.4}Sr_{0.6}Ti_{1-y}Co_yO_{3\pm\delta}$ materials the formal valence of Ti stays close to 4+ for all compositions, whereas the local atomic and electronic structures around Co change dramatically as a function of y . According to our DFT calculations, the structural changes around Co deduced from the EXAFS data have a very strong effect on the Co K-edge. The direct determination of the Co valence from the Co K-edge position is therefore not possible in the present case. However, the comparison to reference materials allows to establish that the formal valence of Co must be close to 3+ in the studied samples. Based on our experimental results, we conclude that the formation of A-site vacancies is driven by the stability of Ti^{4+} , as its reduction requires a finite energy. Based on this conclusion, we can explain why the A-site deficiency is reduced with increasing Co content and so predict that oxygen vacancies will be much more easily formed in $La_{0.4}Sr_{0.6}Ti_{1-y}Co_yO_{3\pm\delta}$ at large Co contents. Therefore, it can be expected that the Co-substituted materials will exhibit an enhanced electrochemical performance as electrode materials than the Co-free variants.

Acknowledgements

This work has been supported by: the Brazilian Synchrotron Light Laboratory (LNLS) under proposals D04B – XAFS 11743 and XAFS1 – 12800, the Argentinean projects PICT-PAE 2288 and the PRH074 ANPCyT-CONICET and the BMBF-MinCyt binational cooperation agreement AL-10-10. CNEA is gratefully acknowledged for supplying equipment, technical staff and laboratories.

REFERENCES

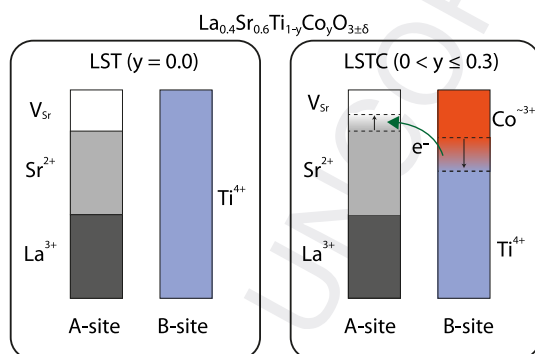


Fig. 6 – Schema representing the charge compensation mechanisms acting in each compositional range and their correlation. Each vertical bar represents the accumulative proportion of each element into a fully occupied perovskite A or B site. a) In the undoped sample, B site is fully occupied by Ti^{4+} while A-site has 20% of vacancies. b) For low cobalt doping level, the electrons provided by the addition of Co into the B-site is used to decrease A-site vacancies.

- [1] Ruiz-Morales JC, Canales-Vázquez J, Peña-Martínez J, López DM, Núñez P. On the simultaneous use of $La_{0.75}Sr_{0.25}Cr_{0.5}Mn_{0.5}O_{3-\delta}$ as both anode and cathode material with improved microstructure in solid oxide fuel cells. *Electrochim Acta* 2006;52:278–84.
- [2] Ruiz-Morales JC, Canales-Vázquez J, Savani C, Marrero-López D, Zhou W, Irvine JTS. Disruption of extended defects in solid oxide fuel cell anodes for methane oxidation. *Nature* 2006;439:568–71.

- 911 [3] Marina OA, Canfield NL, Stevenson JW. Thermal, electrical,
912 and electrocatalytical properties of lanthanum doped
913 strontium titanate. Solid State Ion 2002;149:21–8.
- 914 [4] Canales-Vázquez J, Ruiz-Morales JC, Marrero-López D, Peña-
915 Martínez J, Núñez P, Gómez-Romero P. Fe-substituted (La, Sr)
916 TiO₃ as potential electrodes for symmetrical fuel cells (SFCs).
917 J Power Sources 2007;171:552–7.
- 918 [5] Ruiz-Morales JC, Marrero-López D, Canales-Vázquez J,
919 Irvine JTS. Symmetric and reversible solid oxide fuel cells.
920 RSC Adv 2011;1:1403–14.
- 921 [6] Adler SB. Factors governing oxygen reduction in solid oxide
922 fuel cell cathodes. Chem Rev 2004;104:4791–843.
- 923 [7] Baqué L, Caneiro A, Moreno MS, Serquis A. High performance
924 nanostructured IT-SOFC cathodes prepared by novel
925 chemical method. Electrochim Commun 2008;10:1905–8.
- 926 [8] Li X, Zhao H, Gao F, Chen N, Xu N. La and Sc co-doped SrTiO₃
927 as novel anode materials for solid oxide fuel cells.
928 Electrochim Commun 2008;10:1567–70.
- 929 [9] Miller DN, Irvine JTS. B-site doping of lanthanum strontium
930 titanate for solid oxide fuel cell anodes. J Power Sources
931 2011;196:7323–7.
- 932 [10] Li X, Zhao H, Zhou X, Xu N, Xie Z, Chen N. Electrical
933 conductivity and structural stability of La-doped SrTiO₃ with
934 A-site deficiency as anode materials for solid oxide fuel cells.
935 Int J Hydrogen Energ 2010;35:7913–8.
- 936 [11] Imada M, Fujimori A, Tokura Y. Metal-insulator transitions.
937 Rev Mod Phys 1998;70:1039–263.
- 938 [12] Ovalle A, Ruiz-Morales JC, Marrero-López D, Canales-
939 Vázquez J, Irvine JTS. Mn-substituted titanates as efficient
940 anodes for direct methane SOFCs. Solid State Ion
941 2006;177:1997–2003.
- 942 [13] Zhao H, Gao F, Li X, Zhang C, Zhao Y. Electrical properties of
943 yttrium doped strontium titanate with A-site deficiency as
944 potential anode materials for solid oxide fuel cells. Solid
945 State Ion 2009;180:193–7.
- 946 [14] Napolitano F, Lamas D, Soldati A, Serquis A. Synthesis and
947 structural characterization of Co-doped lanthanum
948 strontium titanates. Int J Hydrogen Energ 2012;37:18302–9.
- 949 [15] Martínez-Coronado R, Aguadero A, Pérez-Coll D, Troncoso L,
950 Alonso JA, Fernández-Díaz MT. Characterization of
951 La_{0.5}Sr_{0.5}Co_{0.5}Ti_{0.5}O_{3-δ} as symmetrical electrode material for
952 intermediate-temperature solid-oxide fuel cells. Int J
953 Hydrogen Energ 2012;37:18310–8.
- 954 [16] Ankudinov AL, Bouldin CE, Rehr JJ, Sims J, Hung H. Parallel
955 calculation of electron multiple scattering using Lanczos
956 algorithms. Phys Rev B 2002;65:104107.
- 957 [17] Meyer GM, Nelmes RJ, Hutton J. High-resolution (direct
958 space) studies of anharmonic motion associated with the
959 structural phase transition in Sr Ti O₃. Ferroelectrics
960 1978;21:461–2.
- 961 [18] Wold A, Ward R. Perowskite-type oxides of cobalt, chromium
962 and vanadium with some rare earth elements. J Am Chem
963 Soc 1954;76:1029–30.
- 964 [19] Blaha P, Schwarz K, Madsen GKH, Kvasnicka D, Luitz J. In: An
965 augmented plane wave + local orbitals program for
966 calculating crystal properties. Austria: Techn. Universitat
967 Wien; 2001.
- 968 [20] Ramallo-López JM, Lede EJ, Requejo FG, Rodriguez JA, Kim J-
969 Y, Rosas-Salas R, et al. XANES characterization of extremely
970 nanosized metal-carbonyl subspecies (Me = Cr, Mn, Fe, and
971 Co) confined into the mesopores of MCM-41 materials. J Phys
972 Chem B 2005;108:20005–10.
- 973 [21] Capehart TW, Herbst JF, Mishra RK, Pinkerton FE. X-ray-
974 absorption edge shifts in rare-earth transition-metal
975 compounds. Phys Rev B 1995;52:7907.
- 976 [22] Berry FJ, Gancedo JR, Marco JF, Ren X. Synthesis and
977 characterization of the reduction properties of cobalt-
978 substituted lanthanum orthoferrites. J Solid State Chem
979 2004;177:2101–14.
- 980 [23] Vashook V, Franke D, Zosel J, Vasylechko L, Schmidt M,
981 Guth U. Electrical conductivity and oxygen nonstoichiometry
982 in the double B mixed La_{0.6}Ca_{0.4}Mn_{1-x}Co_xO_{3-δ}[δ]
983 perovskite system. J Alloy Compd 2009;487:577–84.
- 984 [24] Itoh T, Nakayama M. Using in situ X-ray absorption
985 spectroscopy to study the local structure and oxygen ion
986 conduction mechanism in (La_{0.6}Sr_{0.4})(Co_{0.2}Fe_{0.8})O_{3-δ}. J Solid
987 State Chem 2012;192:38–46.
- 988 [25] Soldati A, Baqué L, Napolitano F, Serquis A. Cobalt-Iron red-
989 ox behavior in nano-structured La_{0.4}Sr_{0.6}Co_{0.8}Fe_{0.2}O_{3-δ}
990 cathodes. J Solid State Chem 2013;189:253–61.
- 991 [26] Krivokapic I, Zerara M, Daku ML, Vargas A, Enachescu C,
992 Ambrus C, et al. Spin-crossover in cobalt(II) imine
993 complexes. Coord Chem Rev 2007;251:364–78.
- 994 [27] Li X, Zhao H, Xu N, Zhou X, Zhang C, Chen N. Electrical
995 conduction behavior of La, Co co-doped SrTiO₃ perovskite as
996 anode material for solid oxide fuel cells. Int J Hydrogen Energ
997 2009;34:6407–14.
- 998 [28] Eror NG, Balachandran U. Self-compensation in lanthanum-
999 doped strontium titanate. J Solid State Chem 1981;40:85–91.
- 1000 [29] Hashimoto S, Kindermann L, Larsen PH, Poulsen FW,
1001 Mogensen M. Conductivity and expansion at high
1002 temperature in Sr_{0.7}La_{0.3}TiO_{3-δ} prepared under reducing
1003 atmosphere. J Electroceram 2006;16:103–7.
- 1004 [30] Hashimoto S, Kindermann L, Poulsen FW, Mogensen M. A
1005 study on the structural and electrical properties of
1006 lanthanum doped strontium titanate prepared in air. J Alloy
1007 Compd 2005;397:245–9.
- 1008 [31] Hui S, Petric A. Electrical conductivity of Yttrium doped
1009 SrTiO₃: influence of transition metals additives. Mater Res
1010 Bull 2002;37:1215–31.
- 1011 [32] Fagg DP, Kharton VV, Kovalevsky AV, Viskup AP,
1012 Naumovich EN, Fraide JR. The stability and mixed
1013 conductivity in La and Fe doped SrTiO₃ in the search for
1014 potential SOFC anode materials. J Eur Ceramic Soc
1015 2001;21:1831–5.
- 1016 [33] Caneiro A. Measurement and regulation of oxygen content in
1017 selected gases using solid electrolyte cells. IV. Accurate
1018 preparation of CO₂–CO and H₂O–H₂ mixtures. J Appl
1019 Electrochemistry 1981;11:83.
- 1020 [34] Caneiro A, Bavadz P, Fouletier J, Abriata JP. Adaptation of an
1021 electrochemical system for measurement and regulation of
1022 oxygen partial pressure to a symmetrical thermogravimetric
1023 analysis system developed using a Cahn 1000 electrobalance.
Rev Scientific Instruments 1982;53:1072.
- 1024 [35] Prado F, Grunbaum N, Caneiro A, Manthiram A. Effect of
1025 La³⁺ doping on the perovskite-to-brownmillerite
1026 transformation in Sr_{1-x}La_xCo_{0.8}Fe_{0.2}O_{3-δ} (0 < x < = 0.4).
Solid State Ion 2004;167:147–54.
- 1027 [36] Oriksa Y, Ina T, Nakao T, Mineshige A, Amezawa K, Oishi M,
1028 et al. X-ray absorption spectroscopic study on
1029 La_{0.6}Sr_{0.4}CoO_{3-δ} cathode materials related with oxygen
1030 vacancy formation. J Phys Chem C 2011;115:16433–8.
- 1031 [37] Berry FJ, Marco JF, Ren X. Reduction properties of phases in
1032 the system La_{0.5}Sr_{0.5}MO₃ (M = Fe, Co). J Solid State Chem
1033 2005;178:961–9.
- 1034 [38] Piovano A, Agostini G, Frenkel AI, Bertier T, Prestipino C,
1035 Ceretti M, et al. Time resolved in situ XAFS study of the
1036 electrochemical oxygen intercalation in SrFeO_{2.5}
1037 brownmillerite structure: comparison with the homologous
1038 SrCoO_{2.5} system. J Phys Chem-US 2011;115:1311–22.